

Modeling of Tsunami Propagation in the Atlantic Ocean Basin for Tsunami Hazard Assessment along the North Shore of Hispaniola*

Annette R. Grilli¹, Stéphan T. Grilli¹, Eric David² and Christophe Coulet²

(1) Department of Ocean Engineering, University of Rhode Island, Narragansett, RI, USA

(2) Artelia, Echirrolles, France

ABSTRACT

Since the devastating earthquake of 2010 in Haiti, significant efforts were devoted to estimating future seismic and tsunami hazard in Hispaniola. In 2013, the UNESCO commissioned initial modeling studies to assess tsunami hazard along the North shore of Hispaniola (NSOH), which is shared by the Republic of Haiti (RH) and the Dominican Republic (DR). This included detailed tsunami inundation for two selected sites, Cap-Haitien in RH and Puerto Plata in DR. This work is reported here.

In similar work done for critical areas of the US east coast (under the auspice of the US National Tsunami Hazard Mitigation Program), the authors have modeled the most extreme far-field tsunami sources in the Atlantic Ocean basin. These included: (i) an hypothetical M_w 9 seismic event in the Puerto Rico Trench; (ii) a repeat of the historical 1755 M_w 9 earthquake in the Azores convergence zone; and (iii) a hypothetical 450 km³ flank collapse of the Cumbre Vieja Volcano (CVV) in the Canary Archipelago. Here, we perform tsunami hazard assessment along the NSOH for these 3 far-field sources, plus 2 additional near-field coseismic tsunami sources: (i) a M_w 8 earthquake in the western segments of the nearshore Septentrional fault, as a repeat of the 1842 event; and (ii) a M_w 8.7 earthquake occurring in selected segments of the North Hispaniola Thrust Fault (NHTF).

Based on each source parameters, the initial tsunami elevation is modeled and then propagated with FUNWAVE-TVD (a nonlinear and dispersive long wave Boussinesq model), in a series of increasingly fine resolution nested grids (from 1 arc-min to 200 m) based on a one-way coupling methodology. For the two selected sites, coastal inundation is computed with TELEMAC (a Nonlinear Shallow Water long wave model), in finer resolution (down to 30 m) unstructured nested grids. Although a number of earlier papers have dealt with each of the potential far-field tsunami sources, the modeling of their impact on the NSOH as well as that of the near-field sources, presented here as part of a comprehensive tsunami hazard assessment study, are novel.

INTRODUCTION

On January 12, 2010, a devastating M_w 7 earthquake struck the Republic of Haiti (RH), causing over 230,000 fatalities, in great part because neither the authorities nor the population were prepared for such a large

magnitude event. The earthquake caused a small local tsunami that added to the destruction and casualties on Haiti's west shore (Fig. 1). Since this catastrophic event, many efforts were devoted to better characterizing seismic hazard in Hispaniola, in order to prepare for and mitigate the impact of future large events. Of particular concern was the tsunami hazard along the north shore of Hispaniola (NSOH) resulting from future large seismic events, both locally and regionally (Fig. 1c). The NSOH is skirted by one of the major faults of Hispaniola, the near-shore Septentrional fault (SF), and the North Hispaniola Thrust fault (NHTF) which runs parallel to it further north (Fig. 1b). In 1842, Haiti's north shore, and particularly the cities of Cap-Haitien and Port-de-Paix, were struck by an earthquake with an estimated M_w 7.6 to 8.1 magnitude; a tsunami was triggered. Both the earthquake and tsunami caused extensive destruction of Haiti's north shore and the area east of it, which nowadays constitutes the north shore of the Dominican Republic (DR); the earthquake caused 5000 fatalities and the tsunami another 300.

In July 2013, a group of experts met in Port-au-Prince, as part of a workshop to assess: "Earthquake and Tsunami Hazard in Northern Haiti: Historical Events and Potential Sources". They issued a proceedings to serve as a basis for performing earthquake and tsunami hazard assessment and risk reduction projects in the area (UNESCO, 2013). The proceedings discusses the source of the 1842 event and those of other earthquakes and tsunamis that could impact Haiti's north shore. In the near-field, several faults or fault segments are identified that could generate large potentially tsunamigenic earthquakes (Fig. 1b). Non-seismic sources of tsunamis in northern Haiti are also considered (e.g., submarine landslides). Based on this work and findings, UNESCO commissioned an initial tsunami hazard assessment study along the entire NSOH, regionally, but also locally in greater details for two selected critical sites, one in RH, Cap-Haitien, and one in DR, Puerto Plata. This paper reports on these initial efforts.

Since 2010, under the auspice of the US National Tsunami Hazard Mitigation Program (NTHMP), the two lead authors have performed tsunami modeling work to develop tsunami inundation maps for the most critical or vulnerable areas of the US east coast (USEC). This has led to selecting and modeling the most extreme far-field tsunami sources, both historical and hypothetical, in the Atlantic Ocean basin, without consideration for their return period or probability. These included: (i) *far-field seismic* sources (Fig. 1a): (1) a series of M_w 9 sources in the Azores con-

*To appear in *Proc. of ISOPE 2015 Intl. Conf. (Kona, HI, June 2015)*

vergence zone, representing possible sources of the 1755 Lisbon earthquake (LSB), and (2) a M_w 9 source in the Puerto Rico Trench (PRT; e.g., Grilli et al., 2010); (ii) a *far-field extreme flank collapse* (450 km³ volume) of the Cumbre Vieja Volcano (CVV) on La Palma (Canary Islands, Fig. 1a; e.g., Abadie et al., 2012; Harris et al., 2012, 2015); and (iii) *near-field Submarine Mass Failures* (SMFs) on or near the USEC continental shelf break (e.g., Grilli et al., 2014).

Here, we simulate tsunami generation and propagation to the NSOH from these far-field tsunami sources and, based on recommendations of UNESCO (2013), from two additional relevant near-field seismic sources: (i) a M_w 8 earthquake in the western segments of the SF, as a repeat of the 1842 event; and (ii) an hypothetical M_w 8.7 earthquake occurring in selected segments of the NHTF. No near-field SMF sources were considered in this initial study, but could be the object of future work. Although a number of earlier papers have dealt in detail with each of the selected far-field tsunami sources (see list above), or have studied tsunami hazard from some near-field seismic sources around Hispaniola (e.g., ten Brink et al., 2008; Calais et al., 2010), to our knowledge, the comprehensive modeling of coastal tsunami hazard from these sources on the NSOH reported here, is novel. Details of numerical models and methodology are given in the next section, followed by details of source selection/parametrization and results of simulations.

TSUNAMI PROPAGATION AND INUNDATION MODELING

Numerical Models

Tsunami propagation from each source to the NSOH is modeled using the nonlinear and dispersive two-dimensional (2D) Boussinesq long wave model (BM) FUNWAVE-TVD, in a series of nested grids of increasing resolution, by way of a one-way coupling method. FUNWAVE-TVD is a newer implementation of FUNWAVE (Wei et al., 1995), which is fully nonlinear in Cartesian grids (Shi et al., 2012) and weakly nonlinear in spherical grids (Kirby et al., 2013). The model was efficiently parallelized for use on a shared memory cluster (over 90% scalability is typically achieved), which allows easily using large grids. FUNWAVE has been widely used to simulate tsunami case studies (e.g., Days et al., 2005; Grilli et al., 2007; Ioualalen et al., 2007; Tappin et al., 2008, 2014; Abadie et al., 2012; Harris et al., 2012, 2015; Grilli et al., 2010, 2013, 2014). The two lead authors have used this model and related methodology to compute tsunami inundation maps for the USEC, as part of the NTHMP work mentioned above (e.g., Abadie et al., 2012; Grilli and Grilli, 2013a; Grilli et al., 2014; Harris et al., 2015; see <http://chinacat.coastal.udel.edu/nthmp.html>) and also for several other tsunami hazard assessment studies of coastal nuclear power plants in the U.S. Both spherical and Cartesian versions of FUNWAVE-TVD were validated through benchmarking and approved for NTHMP work.

As they include frequency dispersion effects, BMs simulate more complete physics than models based on Nonlinear Shallow Water Equations (NSWE), which until recently were traditionally used to model coseismic tsunami propagation. Dispersion is key to accurately simulating landslide tsunamis, which usually are made of shorter and hence more dispersive waves than for coseismic tsunamis (Watts et al., 2003). However, including dispersion is also key to modeling propagation and coastal impact of coseismic tsunamis, as considered here except for CVV, since dispersive shock waves (a.k.a, undular bores) can be generated near the crest of incoming long waves in increasingly shallow water (Madsen et al., 2008). The importance of dispersion in modeling tsunami propagation was confirmed by running FUNWAVE in both BM and NSWE modes, by Tappin et al. (2008) for the 1998 Papua New Guinea landslide tsunami, and by Ioualalen et al. (2007) for the 2004 Indian Ocean and Kirby et al. (2013) for the 2011 Tohoku, coseismic tsunamis. See also Glimsdal et al. (2013) for a recent discussion.

The initial tsunami elevation of both far- and near-field seismic

sources (LSB, PRT, SF, NHTF) to be used in FUNWAVE-TVD is obtained using Okada's (1985) method, based on fault plane parameters (see details later), which computes the seafloor deformation caused by a dislocation in a fault plane embedded in a homogeneous semi-infinite half-space. Assuming that water is incompressible and raise time is small, seafloor deformation is used as initial tsunami elevation on the free surface (with no velocity), which defines the "seismic tsunami source".

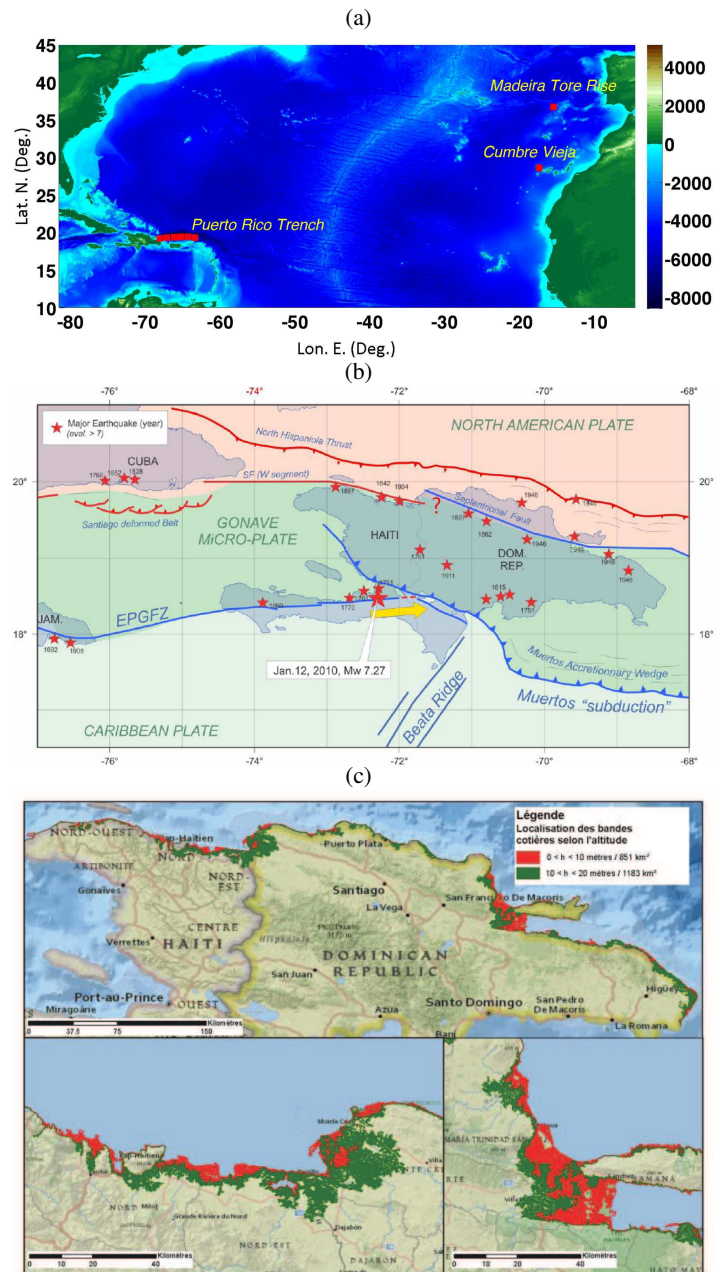


Fig. 1: Tsunami hazard assessment on the North Shore of Hispaniola (NSOH): (a) North Atlantic Ocean Basin with location of far-field tsunami sources and footprint and ETOPO1 bathymetry (meter) of FUNWAVE-TVD 1 arc-min spherical grid G1; (b) Seismo-tectonic context of Hispaniola, with locations of major faults/near-field tsunami sources (NHTF and SF) (from UNESCO, 2013) (c) Geography of RH, DR and the NSOH, with locations of vulnerable sites and critical infrastructures (coastal areas below 10 m elevation are marked in red and those between 10 and 20 meter elevations are marked in green); Cap Haitien and Puerto Plata are two sites finely modeled in this work.

Tsunami generation by the subaerial slide triggered by the CVV flank collapse was simulated by Abadie et al. (2012), using a multi-material

three-dimensional (3D) Navier-Stokes (NS) model, in which the slide was represented as a heavy Newtonian fluid (Abadie et al., 2010); we will use results of Abadie et al.'s 3D-NS model (THETIS) to initialize FUNWAVE-TVD, as a surface elevation and depth averaged current computed after tsunami generation has fully occurred (here after 20 min). In the NTHMP-USEC work, tsunami generation by SMFs, assumed to be rigid slumps or slides, was modeled using the 3D non-hydrostatic σ -coordinate model NHWAVE (Ma et al., 2012; Grilli et al., 2014); in the results presented here, however, no SMF source was considered, but these could be modeled in future work with the same approach.

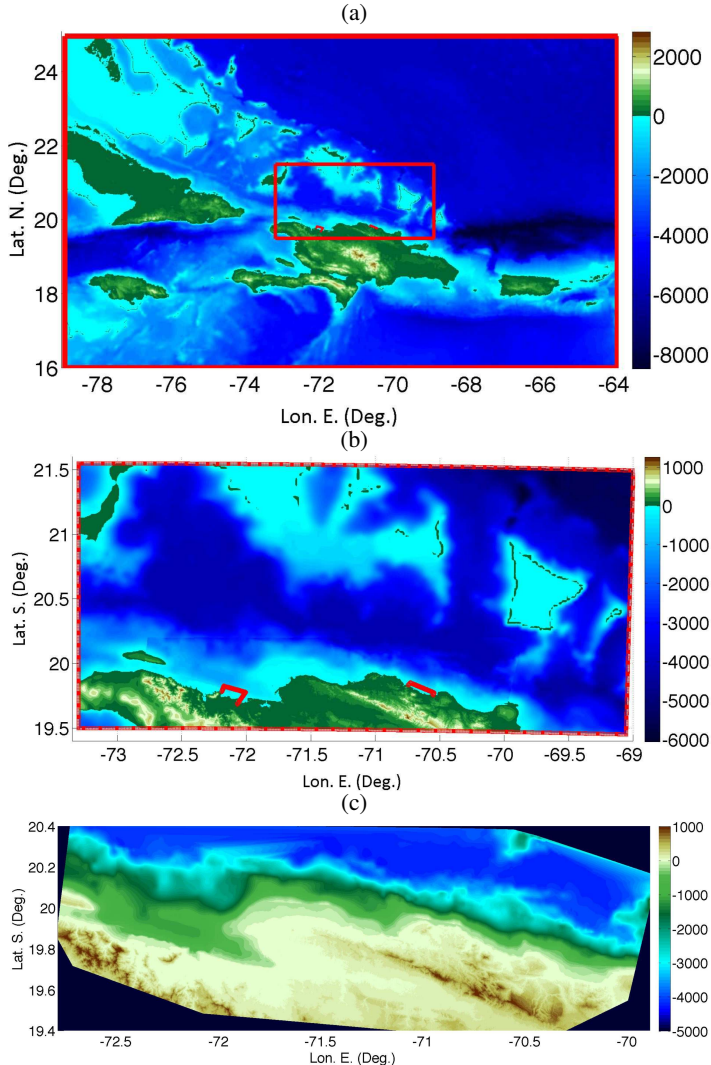


Fig. 2: Tsunami hazard assessment on the North Shore of Hispaniola (NSOH). Footprint and topography of FUNWAVE-TVD: (a) 20 arc-sec spherical grid G2 (red box marks boundary of G22a grid); (b) 205 m Cartesian grid G22a used for far-field source modeling (red boxes mark boundary of irregular mesh (12-30 m) used with TELEMAC in Cap Haiti and Puerto Plata); and (c) Digitized 30 m bathymetry from maritime charts and land maps. Red dots in (a,b) mark locations of stations in the one-way-coupling method. Color scale is bathymetry (meter), from 1 arc-min ETOPO1 data and 30 m nearshore DEM.

Although coseismic tsunamis in deep water can often be approximated by linear non-dispersive waves, they transform into more complex nonlinear and dispersive wave trains as they propagate into shallower water. As indicated before, dispersive shock waves often appear in shallow water near the crest of long incident waves (Madsen et al., 2008; Grilli et al. 2014). Higher frequency waves in such complex wave trains end up breaking near- and on-shore similar to long ocean swell, while

being carried by longer tsunami waves that cause the brunt of the inundation. FUNWAVE-TVD features the relevant physics to accurately simulate such processes, given enough resolution, and its computational efficiency allows computing the entire propagation and coastal impact with dispersion; hence, if the physics calls for it, which is problem dependent, dispersion will be able to express itself through the model equations. Additionally, dissipative processes from bottom friction and breaking waves are well represented in the model, the latter using a front tracking (TVD) algorithm and switching to NSWs in grid cells where breaking is detected (with a breaking criterion). Earlier work shows that numerical dissipation in NSW models closely approximates the physical dissipation in breaking waves (Shi et al., 2012).

Accordingly, as dispersion no-longer matters at this stage of coastal impact, computations of onshore inundation in Cap Haiti and Puerto Plata are performed using TELEMAC (<http://www.opentelemac.org/>), which solves NSWs on an unstructured triangular grid (12-30 m size range), forced by results of FUNWAVE-TVD along an offshore boundary (Fig. 2b). Only limited results of this phase of the work are presented here, which is left out for a future publication.

Methodology

Simulations of tsunami propagation with FUNWAVE-TVD are performed in nested grids, using a one-way coupling method (Fig. 2), in which time series of surface elevation and depth-averaged current are computed for a large number of stations/numerical wave gages, defined in a coarser grid, along the boundary of the finer grid used in the next level of nesting. Computations are fully performed in the coarser grid and then are restarted in the finer grid using the station time series as boundary conditions. As these include both incident and reflected waves computed in the coarser grid, this method closely approximates open boundary conditions. It was found that a nesting ratio with a factor 3-4 reduction in mesh size allows achieving good accuracy in tsunami simulations. Note that to prevent reflection in the first grid level, sponge layers are used along all the offshore boundaries. Along the shore, FUNWAVE-TVD has an accurate moving shoreline algorithm that identifies wet and dry grid cells. Bottom friction is modeled by a quadratic law with a constant friction coefficient (Shi et al., 2012). In the absence of more specific data we used the standard value $C_d = 0.0025$, which corresponds to coarse sand and is conservative as far as tsunami runup and inundation. Earlier work indicates that tsunami propagation results are not very sensitive to friction coefficient values in deeper water.

For regional inundation mapping caused by the 3 far-field sources (LSB, PRT, CVV), simulations are initiated in an ocean basin scale grid, with a 1 arc-min resolution spherical grid G1 (about 1800 m), covering the footprint of Fig. 1a (with 100 to 200 km wide sponge layers), where the far-field tsunami sources are specified as initial conditions. The second level of nesting is a regional 20 arc-sec grid G2 (about 500-600 m; Fig. 2a), which is followed by a third level Cartesian grid G22a with a 205 m resolution (Fig. 2b). For the 2 near-field tsunami sources, simulations directly start in 205 m resolution Cartesian grids G22b,c (with 20 to 50 km wide sponge layers), which have a footprint close to that shown in Fig. 2b. The initial surface elevation and velocity of each tsunami source are specified in FUNWAVE-TVD's first grid level.

For each grid level, whenever possible, bathymetry and topography are interpolated from data of accuracy commensurate with the grid resolution. In deeper water, we use NOAA's 1 arc-min ETOPO-1 data (Figs. 1a and 2a). In shallower water and on continental shelves, since no finer resolution Digital Elevation Maps (DEMs) were publicly available along the NSOH (as, e.g., in the U.S., NOAA's NGDC 3" and 1" Coastal Relief Model data), we created a 30 m resolution DEM by digitizing maritime charts and land maps (Fig. 2c).

RESULTS

Source parameters, tsunami generation, and oceanic propagation

Here, we give results of the parametrization, initialization and initial propagation in FUNWAVE-TVD's 1 arc-min grid G1 (Fig. 1a), of the 3 far-field sources (LSB, PRT and CVV). We also provide results of the parametrization and initialization of the 2 near-field seismic sources (NHTF and SF) in the regional grids G22a,b,c.

For the seismic sources the required parameters of Okada's (1985) method include a fault plane area (width W and length L), depth at the source centroid, centroid location (lat-lon), 3 angles for orientation of the fault plane (dip, rake, strike) and the shear modulus (μ) of the medium (10-60 Gpa, for shallow rupture in soft/poorly consolidated marine sediment to deep rupture in basalt). The moment magnitude of the anticipated earthquake is defined as M_o (J) = μLWS , where S denotes fault slip. Therefore, besides the geometrical and material parameters, to complete the source parameterization, one needs either the slip value or the M_o value of the considered event (or the magnitude, $M_w = (\log M_o)/1.5 - 6$, on a base 32 log scale).

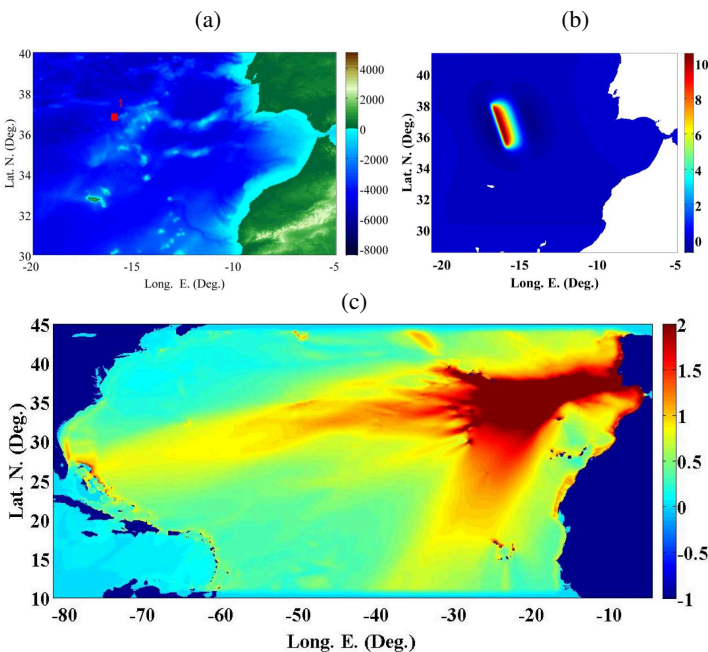


Fig. 3: Far-field tsunami source for M_w 9.0 earthquake in the Azores convergence zone (Madeira Trench Rise; LSB) : (a) Source location and surrounding bathymetry; (b) initial tsunami surface elevation computed with Okada's (1985) method (from Grilli and Grilli, 2013a); and (c) maximum tsunami surface elevation computed with FUNWAVE-TVD in 1 arc-min grid (Fig. 1). [All color scales are in meter.]

For a subduction zone such as PRT, potential slip can be estimated as the convergence rate (e.g., mm/year) times the number of years considered for the event return period. With this approach, Grilli et al. (2010) for instance found that a M_w 9.1 PRT earthquake corresponds to a 600 year return period, while a M_w 8.1 earthquake to only 40 years. For the onshore or offshore faults near Hispaniola (NHTF and SF), however, one has to rely on other estimates, such as historical seismic records. ten Brink et al. (2008) provide many parameters for tele-seismic sources and some of the regional sources in the North Atlantic and UNESCO (2013) also provides expected maximum magnitudes (of M_w 8.7 and 8.0, respectively) and some fault plane parameters for these events. While the authors have already modeled both far-field seismic sources (LSB and PRT) as part of earlier NTHMP work (Grilli et al., 2010; Grilli and Grilli, 2013a), some source parameters were adjusted here within the geophysical uncertainty to maximize tsunami impact on the NSOH; regional and

local grids also will be different. Similarly, for the near-field seismic sources, parameters will be selected within the geophysical uncertainty to maximize impact on the NSOH and in particular at the two selected critical sites of Cap Haiti and Puerto Plata.

For the only non-seismic source considered here, the CVV flank collapse, assuming the most extreme scenario of 450 km³, FUNWAVE-TVD is initialized based on surface elevation and velocity computed at 20 min after the start of the event by Abadie et al. (2012).

Details of parameterization, tsunami generation, and initial oceanic propagation for each source are given in the following.

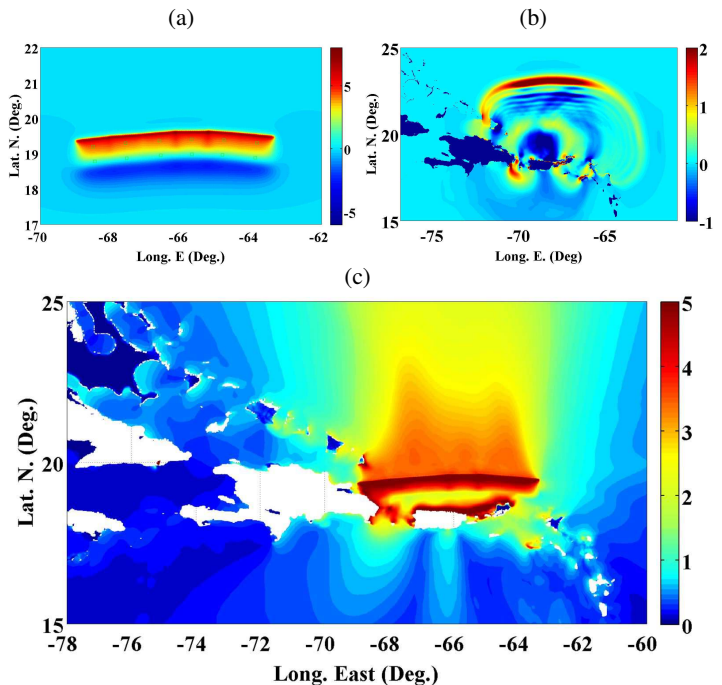


Fig. 4: Far-field tsunami source for M_w 9.0 earthquake in the Puerto Rico Trench (PRT; Grilli et al., 2010) : (a) initial surface elevation computed with Okada's (1985) method; and simulations with FUNWAVE-TVD in 1 arc-min grid (Fig. 1) of (b) instantaneous (30 min) and (c) maximum surface elevations after 3 h of propagation. [All color scales are in meter.]

Far-field LSB source The exact location and parameters of the 1755 LSB event (Fig. 1), which is the basis for this M_w 9 seismic source, are unknown. As part of the NTHMP-USEC work, Grilli and Grilli (2013a) modeled a dozen sources of this magnitude, sited at various locations in the Açores convergence zone, with parameters selected based on earlier published work. Strike angle, in particular, which strongly affects the tsunami directionality, was varied to cause maximum impact on various sections of the USEC. Here, we selected the location and strike angle that caused maximum impact in the Carrabeans and Hispaniola (shown in Figs. 3a,b). The other parameters of the fault plane are (Barkan et al., 2008): (i) fault plane center: -10.753 E Lon. 36.042 N Lat., (ii) $L = 317$ km, (iii) $W = 126$ km, (iv) dip angle: 40 deg., (v) rake angle: 90 deg., (vi) strike angle: 345 deg.; (vii) $S = 20$ m, and (viii) $\mu = 40$ GPa, which yields $M_o = 3.162 \cdot 10^{22}$ J or $M_w = 9$. Using these parameters in Okada's model, we find the initial surface elevation shown in Fig. 3b.

Propagating this source with FUNWAVE-TVD in grid G1, after 9 h, we find the maximum tsunami surface elevation plotted in Fig. 3c. Maximum tsunami impact is clearly aimed at the area of the NSOH; in this coarse grid, maximum elevations appear to be on the order of 1 m.

Far-field PRT source As in Grilli et al. (2010), we are modeling an extreme $M_w = 9$ seismic source in the PRT, corresponding to the entire

trench rupturing north of Puerto Rico (Figs. 1,4), over a 600 km length. Unlike in this earlier work, where only one fault plane was used, to better model the curved geometry of the trench, we use 12 individual sub-fault planes with parameters obtained from the SIFT data base (“Short-term Inundation Forecast for Tsunamis”; Gica et al., 2008). Each sub-fault corresponds to a so-called SIFT unit source of magnitude $M_w = 7.5$, length $L = 100$ km, width $W = 50$ km and a slip of 1 m; with these parameters, one can show that $\mu = 35.6$ GPa. Moreover the location, depth and orientation of each subfault plane (strike, dip and rake angles) is based on the local geology (see details in Grilli and Grilli, 2013b). The slip of each subfault is scaled for the total magnitude to be $M_w = 9$, or $M_o = 3.162 \cdot 10^{22}$ J; thus, $S = (M_o/12)/(LW\mu) = 14.8$ m. Using these parameters in Okada’s model, we find the initial surface elevation shown in Fig. 4a, which varies between -6 and +8 m. Fig. 4b shows the surface elevation after 30 min of propagation of this source with FUNWAVE-TVD, in grid G1. We see a fairly narrow and directional train of the largest tsunami waves aimed almost directly north (at the upper USEC; see Grilli et al., 2010), with some westward propagation affecting the NSOH, with elevations of order 1 m. The maximum tsunami surface elevation after 3 h of propagation is plotted in Fig. 4c; while in this coarse grid, most of the NSOH would experience up to 1.5 m surface elevation, the eastern end of the coast would be impacted by much larger waves, up to 5 m elevation.

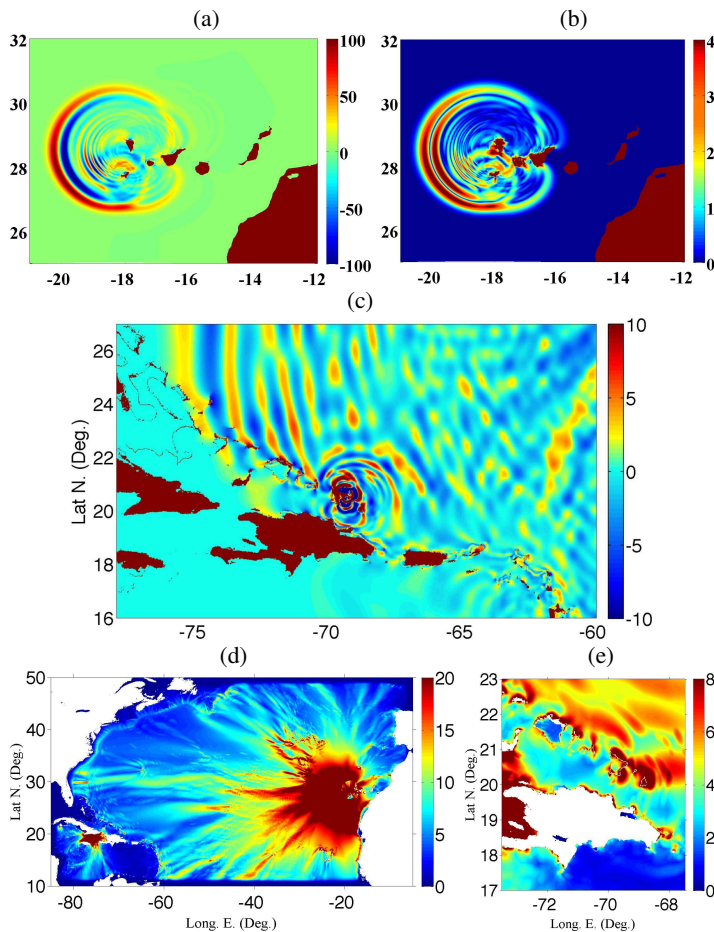


Fig. 5: Far-field tsunami source for 450 km^3 Cumbre Vieja Volcanic flank collapse (CVV): (a,b) source elevation (meter) and velocity module (m/s) after 20 min (Abadie et al., 2012; Harris et al., 2014); surface elevation (meter) computed with FUNWAVE-TVD in 1 arc-min grid (Fig. 1), (c) instantaneous after 7h20', (d,e) maximum over 8 h of simulations. [The very large elevations in (d,e) west of Hispaniola are spurious and due to grid coarseness; these disappear in finer nested grids.]

Far-field volcanic collapse source (CVV) The surface elevation and velocity of the 450 km^3 CVV flank collapse source (from Abadie et al., 2012) are shown in Figs 5a,b, 20 min after the event; at that time, we see a concentric wave train with elevations ranging between -100 and +100 m, velocity modules up to 4 m/s, and a clear directionality in the WSW direction. Fig. 5c shows the instantaneous surface elevation around Hispaniola, after 7 h 20 min of propagation computed with FUNWAVE-TVD in grid G1. Despite the long propagation distance, very large waves with elevations in the range -10 m to +10 m are approaching the NSOH. The maximum tsunami surface elevation after 8 h of propagation is plotted in Figs. 5d,e; in this coarse grid, most of the NSOH would experience up to 4 to 8 m surface elevation. It should be noted that the very large elevations in (d,e) west of Hispaniola are spurious and due to grid coarseness; these disappear in finer nested grids.

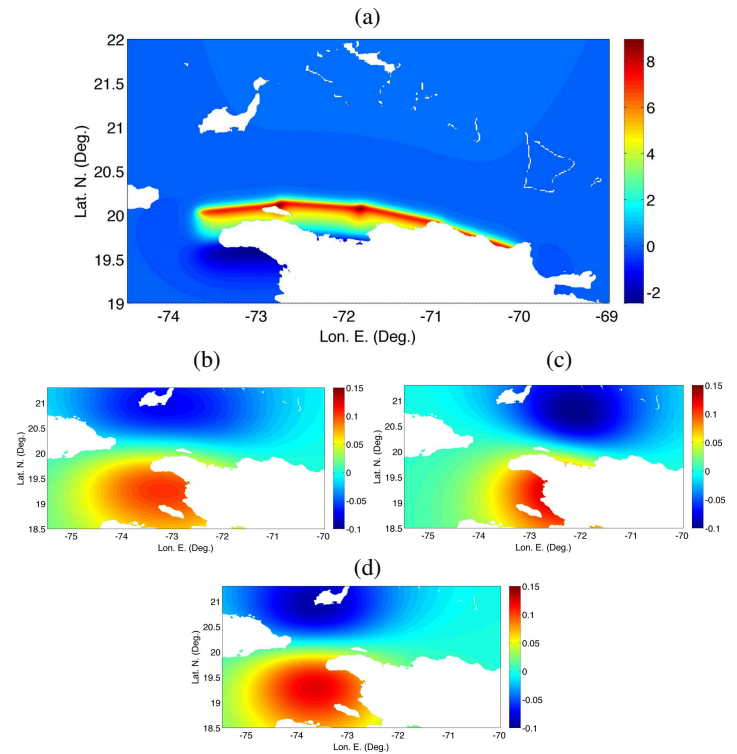


Fig. 6: Near-field seismic tsunami sources, initial surface elevation computed with Okada’s method for: (a) a $M_w 8.7$ earthquake in the NHTF; (b,c,d) three scenarios (#1,2,3) of a $M_w 8$ earthquake in the SF. [All color scales in meter.]

Near-field seismic sources (NHTF, SF) For the near-field source in NHTF, UNESCO (2013) recommends a 45 deg. dip angle; however, local SIFT sources use a 20 deg. angle, which will cause greater tsunami generation. Hence, this shallower value of dip is used here, together with other parameters specified for 4 local (100 by 50 km) unit SIFT sources, covering the fault area (Fig. 6a); the unit SIFT sources used are referred to as B55 to B58 in NOAA’s database. Despite the shallow depth of the fault plane (5 km), because we are near a deep subduction zone, we use the standard value $\mu = 35.6$ GPa, which to achieve the $M_w 8.7$ magnitude of the source (or $M_o = 1.122 \cdot 10^{22}$ J) leads to a slip $S = (M_o/4)/(LW\mu) = 15.76$ m. In the corresponding initial source computed with Okada’s method in Fig. 6a, the surface elevation varies in the range -2.5 to +9 m, which owing to the proximity of the NHTF should cause a significant tsunami impact on the NSOH.

In Fig. 1b, we see that the SF is approximately 300 km long, and is in an more or less E-W direction from east of Cuba, (strike angle of 90 deg.) to Turtle Island; then it becomes parallel to the NSOH (strike angle of 100 deg.). UNESCO (2013) recommends a 90 deg. dip angle

for this fault. As this is not a subduction zone, and the fault is nearshore and almost vertical, a M_w 8 earthquake could occur under various partial rupture scenarios. Thus, we defined 3 rupture scenarios: #1) 2 segments on the west of the SF, of 170 and 100 km (total length 270 km); #2) 1 segment on the east of the SF of 100 km length; and #3) 1 segment on the west of the SF of length 170 km. For each of these scenarios, we assume a 30 km width and a 85 deg. dip angle (to be conservative). Slip for each scenario is computed the usual way to achieve a magnitude $M_w = 8$ or $M_o = 1.00 \cdot 10^{21}$ J, in each case as: $S = M_o / (LW\mu) = 3.47, 9.37, \text{ and } 5.51$ m, respectively (in the absence of information, we used $\mu = 35.6$ GPa). In the corresponding initial sources computed with Okada's method in Figs. 6b,c,d, the surface elevation varies in the range -0.10 to +0.15 m, which is quite small compared to the other sources and will not cause great impact on the NSOH, despite the proximity of the fault to shore. In simulations, scenario #1 will even be a priori eliminated since it only causes 5 cm initial wave elevations along the NSOH.

Finally, in view of the size of the tsunami impact on the NSOH from most of the other sources, we will also neglect tsunami generation from the rupture of land-locked faults, such as the easternmost part of the SF (Fig. 1b).

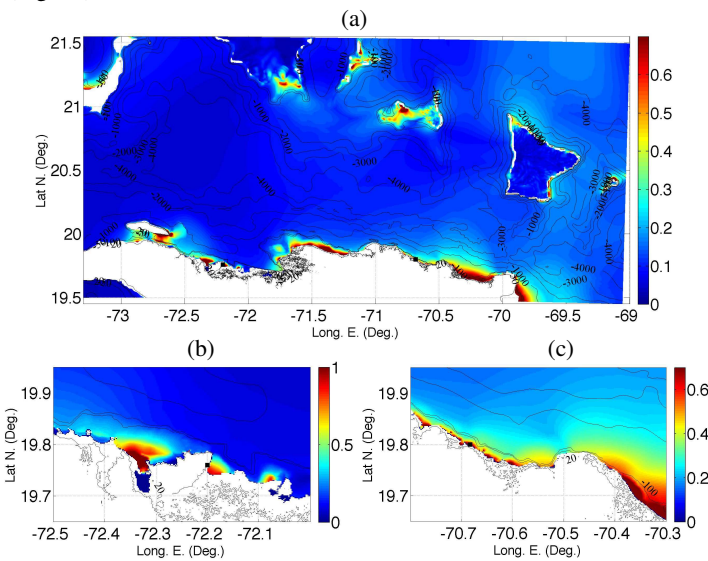


Fig. 7: Far-field LSB M_w 9.0 seismic tsunami source: (a) envelope of maximum surface elevation computed in grid G22a after 9 h of propagation; zoom around (b) Cap Haitien, and (c) Puerto Plata (both marked by a black square). [All color scales are in meter.]

Regional and near-shore tsunami propagation

Here we present, for each far- and near-field source, the envelope of maximum surface elevation computed with FUNWAVE-TVD in the regional Cartesian grids G22a,b,c (205 m resolution). For the far-field sources, these are obtained by one way coupling based on results in G1 and G2 grids, the latter not detailed here). For the near-field sources these are direct results of simulations in the G22 grids.

In all cases, time series of tsunami elevation and current (not shown here) are computed at many stations along the outer boundary of the small 30 m resolution grids located around the two critical sites of Cap Haitien and Puerto Plata (Fig. 2b) to perform additional simulations of coastal flooding with TELEMAC.

Far-field sources Figs. 7, 8, and 9 show the envelopes of maximum surface elevations computed in grid G22a for the LSB, PRT and CVV far-field tsunami sources. In each case, results are shown in panel (a) for the whole grid and in panels (b) and (c) as zoom-ins around the two critical areas of Cap Haitien and Puerto Plata. As expected from earlier

simulations, the maximum coastal impact occurs for the CVV source, with up to 9 to 20 m runup at each of the sites. The next largest impact is caused by the PRT source, with 3 to 4 m runup at the sites, and finally LSB, with only up to 1 and 0.7 m runup at the sites.

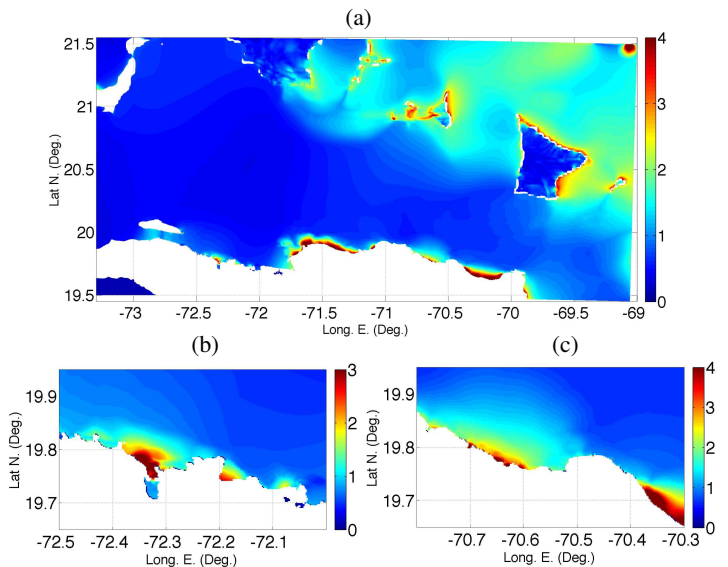


Fig. 8: Far-field PRT M_w 9.0 seismic tsunami source: (a) envelope of maximum surface elevation computed in grid G22a after 3 h of propagation; zoom around (b) Cap Haitien, and (c) Puerto Plata (see locations in Fig. 7). [All color scales are in meter.]

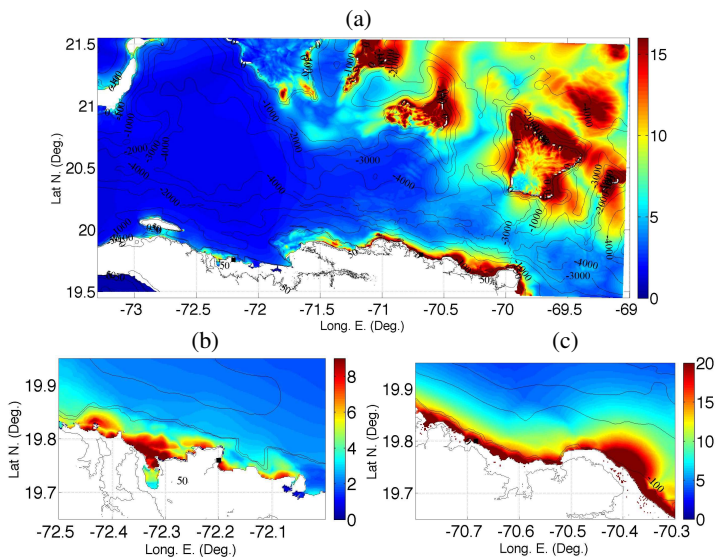


Fig. 9: Far-field CVV 450 km³ flank collapse tsunami source: (a) envelope of maximum surface elevation computed in grid G22a after 8 h of propagation; zoom around (b) Cap Haitien, and (c) Puerto Plata (locations marked by black squares). [All color scales are in meter.]

Near-field sources Figs. 10 and 11 show the envelopes of maximum surface elevations computed in grids G22b and G22c, for the NHTF and SF (scenario #2) near-field tsunami sources, respectively. In each case, results are shown in panel (a) for the whole grid and in panels (b) and (c) as zoom-ins around the two critical areas of Cap Haitien and Puerto Plata. As expected from their initial source, the maximum coastal impact occurs for the NHTF source, with up to 8 to 12 m runup at each of the sites. By contrast, the two scenarios (#2 and #3) modeled for the SF source cause much less impact. Only results for scenario #2 are presented here, which

causes more impact on the NSOH than scenario #3; even though, we only see maximum runups of 0.15 to 0.5 m at each of the sites.

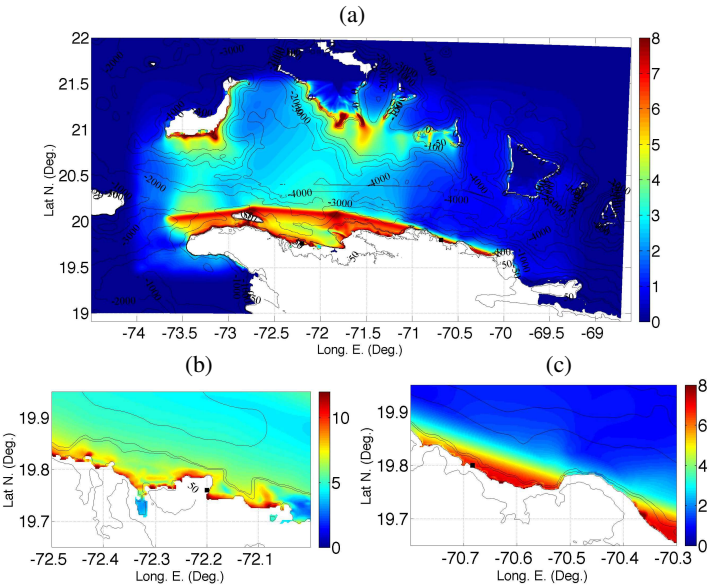


Fig. 10: Near-field NHTF M_w 8.7 seismic tsunami source: (a) envelope of maximum surface elevation computed in grid G22b after 1 h of propagation (note the damping effect of sponge layers around the grid boundary); zoom around (b) Cap Haitien, and (c) Puerto Plata (locations marked by black squares). [All color scales are in meter.]

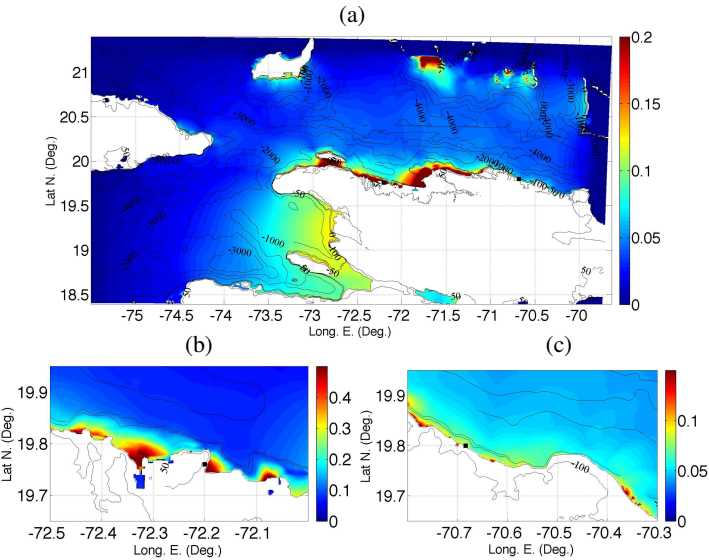


Fig. 11: Near-field SF M_w 8.0 (scenario #2) seismic tsunami source: (a) envelope of maximum surface elevation computed in grid G22c after 1 h of propagation (note the damping effect of sponge layers around the grid boundary); zoom around (b) Cap Haitien, and (c) Puerto Plata (locations marked by black squares). [All color scales are in meter.]

Tsunami coastal impact at the two critical sites

Here, due to lack of space, we only present a few results of the fine grid modeling of tsunami coastal impact, using TELEMAC, at the two selected critical sites of Cap Haitien and Puerto Plata. The grids used, with the footprint shown in Fig. 2, are irregular triangular meshes (12 to 30 m resolution), nested in FUNWAVE-TVD's grids G22a,b,c. For each of the selected tsunami sources (PRT, CVV, NHTF), TELEMAC is forced by time series of surface elevation and currents computed with FUNWAVE-TVD along each fine grid boundary.

The TELEMAC modeling system was developed by a European consortium of partners led by EDF-DRD (Hervouet, 2007) and is dedicated to solving environmental problems in fluid mechanics. The model is more particularly designed for performing flood risk assessments, including coastal inundation from storms and, in the present context, tsunami. TELEMAC-2D solves the 2D St Venant equations (a.k.a NSW equations), which describe the nonlinear temporal and spatial evolution of flow depth and depth-averaged current, including effects of bottom friction. TELEMAC uses a Finite Element Method on irregular triangular meshes (e.g., see Fig. 12 for Puerto Plata's grid), which more easily allows refining the grid's nearshore resolution in very shallow water and defining unstructured meshes that can follow the terrain features (bathymetry, coastline, port infrastructure, cities and buildings...).

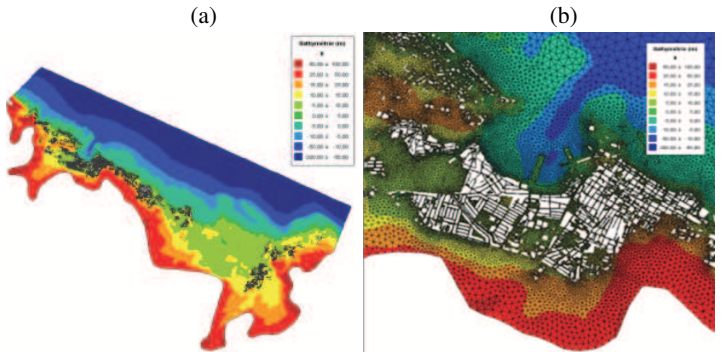


Fig. 12: Irregular FEM grid (12 to 30 m size triangular elements) used with TELEMAC: (a) entire grid around Puerto Plata (footprint of the grid is also shown in Fig. 2b); (b) zoom-in on the center of the city. Note, the mesh includes buildings and infrastructures (i.e., it is not based on a bare land DEM).

Here, TELEMAC is forced at its ocean boundary with results from FUNWAVE-TVD's highest resolution 205 m Cartesian grids. The model then computes tsunami propagation in shallow water, over land, and within the cities at the two critical sites. These more detailed and site specific results of tsunami flow depth and velocity can be used to support decisions with regards to mitigation and future crisis management. Fig 13 shows an example of results of flow depth mapping for the M_w 8.7 NHTF source around Cap Haitien, which also identifies the most vulnerable sites such as administrative buildings, economical areas, schools and churches. The map provides elements that can be used for preliminary crisis management plans, such as evacuation routes, and evacuation areas. Detailed work on this and similar flood mapping, vulnerability assessment, and crisis management plans will be presented and discussed in a future publication led by the third and fourth authors of this paper.

CONCLUSIONS

The tsunami simulations with FUNWAVE-TVD of the selected far- and near-field sources governing tsunami hazard along the NSOH, in nested grids down to a 205 m resolution, provide a synoptic view of the tsunami coastal impact on the NSOH. Thus, we see that, among all the far-field sources, CVV causes by far the largest impact, with up to 20 m runup at the critical sites, followed by PRT, with up to 4 m; impact from a LSB source can be considered as negligible in view of those. A CVV induced tsunami would reach the NSOH after 6.5 h, while a PRT tsunami would start impacting it after 30 min. This short propagation time, coupled to a much shorter return period (a few hundred years compared to over 100,000 years for CVV) make PRT the most dangerous far-field source (in terms of probability of a given impact). In the near-field, the NHTF source, whose return period would be on the order of that of PRT, or even less, dominates tsunami coastal hazard on the NSOH, with up to

12 m runup at the critical sites and propagation times of minutes, thus offering very little warning time.

In view of these results, fine grid (12-30 m resolution) simulations with TELEMAC at the two critical sites were performed only for the CVV, PRT and NHTF sources. Examples of TELEMAC results are provided, in terms of flow depth and vulnerability at Cap Haitien, that can be used to draw evacuation plans and prepare for crisis management. More details in this respect will be reported in a future publication.



Fig. 13: Maximum flow depth computed with TELEMAC around Cap Haitien, in 12-30 m resolution irregular FEM grid (footprint of the grid is also shown in Fig. 2b), for the M_w 8.7 near-field seismic NHTF source.

Acknowledgments This research was supported by UNESCO funding. The authors are solely responsible for the results presented in this paper.

REFERENCES

- Abadie, S., Morichon, D., Grilli, S.T. and S. Glockner (2010). ‘Numerical simulation of waves generated by landslides using a multiple-fluid Navier-Stokes model,’ *Coast. Engng.*, 57, 779-794, doi:10.1016/j.coastaleng.2010.03.003.
- Abadie, S., J.C. Harris, S.T. Grilli and R. Fabre (2012). ‘Numerical modeling of tsunami waves generated by the flank collapse of the Cumbre Vieja Volcano (La Palma, Canary Islands): tsunami source and near field effects,’ *J. Geophys. Res.*, 117, C05030, doi:10.1029/2011JC007646.
- Barkan, R., ten Brick, U.S., Lin, J. (2008). ‘Far field tsunami simulations of the 1755 Lisbon earthquake: Implication for tsunami hazard to the U.S. East Coast and the Caribbean,’ *Marine Geol.*, 264, 109-122.
- Calais, E., A. Freed, G. Mattioli, F. Amelung, S. Jansson, P. Jansma, S.-H. Hong, T. Dixon, C. Prépetit and R. Momplaisir (2010). ‘Transpressional rupture of an unmapped fault during the 2010 Haiti earthquake,’ *Nature Geosc.*, 3, 794-799.
- Day, S. J., P. Watts, S. T. Grilli and Kirby J.T. (2005). ‘Mechanical Models of the 1975 Kalapana, Hawaii Earthquake and Tsunami,’ *Mar. Geol.*, 215(1-2), 59-92.
- Gica, E., M. C. Spillane, V. V. Titov, C. D. Chamberlin, and J. Newman (2008). ‘Development of the forecast propagation database for NOAA’s Short-Term Inundation Forecast for Tsunamis,’ *NOAA Tech. Memo. OAR PMEL-139*.
- Glimsdal S., Pedersen G.K., Harbitz C.B., and Løvholt F. (2013) ‘Dispersion of tsunamis: does it really matter?’ *Nat. Hazards Earth Syst. Sci.*, 13, 1507-1526, doi:10.5194/nhess-13-1507-2013.
- Grilli A.R. and S.T. Grilli (2013a). ‘Modeling of tsunami generation, propagation and regional impact along the U.S. East Coast from the Azores Convergence Zone,’ *Research Report no. CACR-13-04*. NTHMP Award, NA10NWS4670010, US National Weather Service Program Office, 20 pp. <http://www.oce.uri.edu/grilli/grilli-grilli-cacr-13-04>.
- Grilli A.R. and S.T. Grilli (2013b). ‘Modeling of tsunami generation, propagation and regional impact along the upper U.S East coast from the Puerto Rico trench,’ *Research Report no. CACR-13-02*. NTHMP Award, NA10NWS4670010, US National Weather Service Program Office, 18 pp. <http://www.oce.uri.edu/grilli/grilli-grilli-cacr-13-02>.
- Grilli, S.T., Ioualalen, M., Asavanant, J., Shi, F., Kirby, J. and Watts, P. (2007). ‘Source Constraints and Model Simulation of the December 26, 2004 Indian Ocean Tsunami,’ *J. Waterway Port Coast. Oc. Engng.*, 133(6), 414-428.
- Grilli, S.T., S. Dubosq, N. Pophet, Y. Prignon, J.T. Kirby and F. Shi (2010). ‘Numerical simulation and first-order hazard analysis of large co-seismic tsunamis generated in the Puerto Rico trench: near-field impact on the North shore of Puerto Rico and far-field impact on the US East Coast,’ *Nat. Haz. Earth Syst. Sc.*, 10, 2109-2125, doi:10.5194/nhess-2109-2010.
- Grilli, S.T., J.C. Harris, T. Tajalibakhsh, T.L. Masterlark, C. Kyriakopoulos, J.T. Kirby and F. Shi (2013). ‘Numerical simulation of the 2011 Tohoku tsunami based on a new transient FEM co-seismic source: Comparison to far- and near-field observations,’ *Pure Appl. Geophys.*, 170, 1333-1359, doi:10.1007/s00024-012-0528-y.
- Grilli S.T., O’Reilly C., Harris J.C., Tajalli-Bakhsh T., Tehranirad B., Banihashemi S., Kirby J.T., Baxter C.D.P., Eggeling T., Ma G. and F. Shi (2014). ‘Modeling of SMF tsunami hazard along the upper US East Coast: Detailed impact around Ocean City, MD,’ *Nat. Haz.*, 42 pps., doi: 10.1007/s11069-014-1522-8 (published online 11/15/14).
- Harbitz, C.B., Glimsdal S., Bazin S., Zamora N., Lovholt F., Bungum H., Smebye H., Gauer P., and Kjekstad O. (2012). ‘Tsunami hazard in the Caribbean: Regional exposure derived from credible worst case scenarios,’ *Continental Shelf Res.*, 8, 1-23, doi:10.1016/j.csr.2012.02.006.
- Harris, J.C., S.T. Grilli, S. Abadie and T. Tajalibakhsh (2012). ‘Near- and far-field tsunami hazard from the potential flank collapse of the Cumbre Vieja Volcano,’ In *Proc. 22nd Offshore Polar Engng. Conf. (ISOPE12, Rodos, June 17-22, 2012)*, Intl. Soc. of Offshore and Polar Engng., 242-249.
- Harris J.C., Tehranirad B., Grilli A.R., Grilli S.T., Abadie S., Kirby J.T. and F. Shi (2015). ‘Far-field tsunami hazard in the north Atlantic basin from large scale flank collapses of the Cumbre Vieja volcano, La Palma,’ *Pure Appl. Geophys.*, 34 pps. (in revision).
- Hervouet, J.M. (2007). *Hydrodynamics of Free Surface Flows: Modeling with the Finite Element Method*. Wiley Edition, 360 pp.
- Ioualalen, M., Asavanant, J., Kaewbanjak, N., Grilli, S.T., Kirby, J.T. and P. Watts (2007). ‘Modeling the 26th December 2004 Indian Ocean tsunami: Case study of impact in Thailand,’ *J. Geophys. Res.*, 112, C07024, doi:10.1029/2006JC003850.
- Kirby, J.T., Shi, F., Tehranirad, B., Harris, J.C. and S.T. Grilli (2013). ‘Dispersive tsunami waves in the ocean: Model equations and sensitivity to dispersion and Coriolis effects,’ *Ocean Modell.*, 62, 39-55, doi:10.1016/j.oceomod.2012.11.009.
- Ma G., Shi F., Kirby J.T. (2012). ‘Shock-capturing non-hydrostatic model for fully dispersive surface wave processes,’ *Ocean Modell.*, 4344, 2235.
- Madsen P.A., D.R. Fuhrman and H. A. Schaffer (2008) ‘On the solitary wave paradigm for tsunamis,’ *J. Geophys. Res.*, 113, C12012.
- Okada, Y. (1985). ‘Surface deformation due to shear and tensile faults in a half space,’ *Bull. Seismol. Soc. America*, 75(4), 1135-1154.
- Shi, F., J.T. Kirby, J.C. Harris, J.D. Geiman and S.T. Grilli (2012). ‘A High-Order Adaptive Time-Stepping TVD Solver for Boussinesq Modeling of Breaking Waves and Coastal Inundation,’ *Ocean Modell.*, 43-44, 36-51, doi:10.1016/j.oceomod.2011.12.004.
- UNESCO (2013). ‘Earthquake and Tsunami Hazard in Northern Haiti: Historical Events and Potential Sources,’ Meeting of Experts (Port-au-Prince, Haiti 1011 July 2013). *Workshop Report No. 255*, 32 pp.
- Tappin, D.R., Watts, P., S.T. Grilli (2008). ‘The Papua New Guinea tsunami of 1998: anatomy of a catastrophic event,’ *Nat. Haz. Earth Syst. Sc.*, 8, 243-266. www.nat-hazards-earth-syst-sci.net/8/243/2008/.
- Tappin D.R., Grilli S.T., Harris J.C., Geller R.J., Masterlark T., Kirby J.T., F. Shi, G. Ma, K.K.S. Thingbaijam, and P.M. Maig (2014). ‘Did a submarine landslide contribute to the 2011 Tohoku tsunami?’ *Mar. Geol.*, 357, 344-361 doi: 10.1016/j.margeo.2014.09.043.
- Ten Brink, U., Twichell D., Geist E., Chaytor J., Locat J., Lee H., Buczkowski B., Barkan R., Solow A., Andrews B., Parsons T., Lynett P., Lin J., and M. Sansoucy (2008). ‘Evaluation of tsunami sources with the potential to impact the U.S. Atlantic and Gulf coasts,’ *USGS Administrative report to the U.S. Nuclear Regulatory Commission*, 300 pp.
- Watts P., Grilli S.T., Kirby J.T., Fryer G.J. and D.R. Tappin (2003) ‘Landslide tsunami case studies using a Boussinesq model and a fully nonlinear tsunami generation model,’ *Nat. Haz. Earth Syst. Sc.*, 3, 391-402.
- Wei, J., Kirby, J.T., Grilli, S.T. and Subramanya, R. (1995). ‘A Fully Nonlinear Boussinesq Model for Surface Waves. Part I. Highly Nonlinear Unsteady Waves,’ *J. Fluid Mech.*, 294, 71-92.